cells

MDPI

Article

Single-cell transcriptomics and in vitro lineage tracing reveals differential susceptibility of human iPSC-derived midbrain dopaminergic neurons in a cellular model of Parkinson's disease

Lucia F. Cardo[1*], Jimena Monzón-Sandoval[1*], Zongze Li[1, 2], Caleb Webber[1], Meng Li[2**]**

[1] Dementia Research Institute, School of Medicine, Cardiff University, Hadyn Ellis Building, Maindy Road, Cardiff, CF24 4HQ, UK
[2] Neuroscience and Mental Health Innovation Institute, School of Medicine, Cardiff University, Hadyn Ellis Building, Maindy Road, Cardiff, CF24 4HQ, UK
* Equal contribution
**Correspondence: Caleb Webber, WebberC4@cardiff.ac.uk
Meng Li, lim26@cardiff.ac.uk

Abstract: Advances in stem cell technologies open up new avenues for modelling development and diseases. The success of these pursuits however relies on the use of cells most relevant to those targeted by the disease of interest, for example, midbrain dopaminergic neurons for Parkinson's disease. In the present study, we report the generation of a human induced pluripotent stem cell (iPSC) line capable of purifying and tracing nascent midbrain dopaminergic progenitors and their differentiated progeny via the expression of a Blue Fluorescent Protein (BFP). This was achieved by CRISPR/Cas9 assisted knock-in of BFP and Cre into the safe harbour locus AAVS1 and an early midbrain dopaminergic lineage marker gene LMX1A, respectively. Immunocytochemical analysis and single cell RNA sequencing of iPSC-derived neural cultures confirms developmental recapitulation of the human fetal midbrain and high-quality midbrain cells. By modelling Parkinson's disease-related drug toxicity using 1-Methyl-4-phenylpyridinium (MPP^+), we showed preferential reduction of BFP^+ cells, a finding demonstrated independently by cell death assays and single cell transcriptomic analysis of MPP^+ treated neural cultures. Together, these results highlight the importance of disease relevant cell types in stem cell modelling.

Keywords: CRISPR/Cas9; midbrain dopaminergic neuron; genome editing; human pluripotent stem cell; in vitro differentiation; Parkinson's disease; single cell RNA sequencing

Citation: To be added by editorial staff during production.

Academic Editor: Firstname Lastname

Received: date
Revised: date
Accepted: date
Published: date

1. Introduction

Parkinson's disease (PD) is the second most common neurodegenerative disorder, affecting 2–3% of the population over 65 years of age and with an incidence increase of 5-10 fold in the later decades of life (1). The main pathological features of PD are the loss of midbrain dopaminergic (mDA) neurons in the substantia nigra pars compacta (SNpc), which project to the striatum and cortex. Current treatment for PD is mainly pharmacological intervention to counterbalance the dwindling supply of striatal dopamine and in some cases managed by a type of surgery called deep brain stimulation. However, all current available treatments are palliative, and there is no means to stop disease progression, to cure, or to prevent PD.

Human pluripotent stem cells (PSCs), including embryonic stem cells and induced pluripotent stem cells, can generate unlimited amount of authentic mDA neurons during in vitro differentiation. These in vitro produced mDA cells are amenable for pharmacological and/or gene expression perturbations to mimic PD-related cellular pathologies and thus present a valuable model for elucidating the molecular mechanisms underlying PD and advancing therapeutic development. MDA neural progenitors can now be induced at a high efficiency from hPSCs and clinical trials using such preparations have been approved for PD cell therapy (2-9). However, neuronal derivatives expressing the cardinal mDA markers (eg. PITX3) are often present in much lower proportion relative to the number of progenitors at early stages, either after differentiation in vitro or following transplantation in the rodent brains. For studies aiming to evaluate the effects of drugs or PD pathogenic genetics on mDA neurons and/or late mDA precursors using RNA sequencing approaches, the low neuronal content incurs significant unwanted cellular heterogeneity. Therefore, PSC lines with a genetically engineered cell type-specific fluorescent reporter would facilitate the isolation of desired cell identity using fluorescent activated cell sorter (FACS). For example, a tyrosine hydroxylase (TH)-based reporter system has been employed for purifying dopamine neurons from mixed PSC-derived neuronal cultures and for studying the migration and integration of transplanted cells in the host brains (10-12) or isolating TH-expressing cells after fixation and immunostaining with fluorophore-conjugated antibodies (13, 14). However, TH expression is not limited to SNpc (A9) but also expressed in other catecholaminergic neurons (15), while its late expression in postmitotic cells doesn't meet the requirement for isolating mDA progenitors and for genetic or pharmacological interrogation prior to or during their differentiation into postmitotic mDA neurons. Moreover, there are currently no available hPSC tools designed for genetic tracking of derivatives of mDA progenitors for in-depth investigations into their developmental fate and characteristics other than the immediate neuronal derivatives of mDA.

During development, the specification of mDA fate in ventral midbrain progenitors is marked by the expression of transcription factor LMX1A (16-19). Using CRISPR/Cas9 assisted genome editing technology, we knocked-in a Cre and silent blue fluorescent protein (BFP) expression unit into the LMX1A and AAVS1 locus, respectively, in the KOLF2-C1 human iPSC line (HPSI0114i-kolf_2, https://hpscreg.eu/cell-line/WTSIi018-B, reference 20). We show here that LMX1A$^+$ mDA neural progenitors derived from the tracer lines can be purified based on BFP expression via FACS with BFP expression maintained in their differentiated progeny regardless of their own LMX1A expression status. Single cell RNA sequencing (scRNAseq) analysis confirmed the authenticity of iPSC mDA identity, and preferential vulnerability of BFP$^+$ neurons to toxicity of 1-Methyl-4-phenylpyridinium (MPP$^+$).

2. Materials and Methods

2.1. PSC culture and mDA differentiation

KOLF2-C1 and genome edited KOLF2-C1 derivatives were maintained on Matrigel-coated plates in Essential 8 media (TeSR-E8, Stemcell Technologies). All iPSCs were passaged via manual dissociation using Gentle Cell Dissociation Reagent (Stemcell Technologies) as described previously (21). IPSC differentiation towards mDA fate follows a protocol combining key features of Kriks et al. and Jagger et al.(2-3). Briefly, iPSCs were preplated on growth factor-reduced matrigel in TeSR-E8. Neural differentiation was initiated when cells reached >80% confluence by switching to DMEM-F12/Neurobasal (2:1) supplemented with N2 and B27 (N2B27). For the first 7 days, cultures were supplemented with SB431542 (10μM, Tocris), LDN-193189 (100nM, StemGene), SHH-C24II (200ng/ml, BioTechne) and Purmorphamine (1μM, VWR). LDN was kept until day 11. On day 3 CHIR99021 (3 μM, Cambridge Bioscience) was added to the media until day 13. Cultures were treated with PD0325901 from day 5 to 9 (1μM, Cambridge Bioscience). FGF8a was added from day 11 to day 20 (100ng/ml, Peprotech). Cultures were dissociated at around day 16/17 to single cells using Accutase (Thermo Fisher Scientific) and replated onto poly-

D-lysine/laminin coated plates at a density of 250000 cells/cm^2. B27 without vitamin A (Thermo Fisher Scientific) was used for the first 25 days, followed by B27 (Thermo Fisher Scientific) plus BDNF (10ng/ml, Peprotech), GDNF (10ng/ml, Cell Guidance System), Ascorbic Acid (200μM, Sigma-Aldrich) and DAPT (10μM, Tocris) from day 21 onwards.

Enhanced growth factor containing media was used for FACS purification at day 18 and post-sort culture of sorted BFP$^+$, sorted BFP$^-$ and unsorted sister controls cells. DMEM-F12/Neurobasal basal media was supplemented with normal B27 together with TGFβ3 (1ng/ml, Peprotech), dbcAMP (500μM, Sigma-Aldrich), Ascorbic Acid (200μM), DAPT (10μM) and GDNF and BDNF at 20ng/ml each. The concentration of GDNF and BDNF was reduced to 10ng/ml one week after sorting.

2.2. CRISPR/Cas9 genome editing of human iPSCs

Two rounds of CRISPR/Cas9 genome editing were carried out to generate the LMX1A-Cre/AAVS1-BFP tracer lines. The first round of editing concerns targeted insertion of a BFP expression cassette downstream of loxP flanked puromycin expression unit in the AAVS1 safe harbor locus. In the second-round genome editing, a CRE protein expression cassette was knocked-in into the LMX1A locus. This strategy allows LMX1A dependent expression of Cre, which then removes the floxed puromycin cassette sandwiched between the CAG promoter and BFP-poly A sequence in the AAVS1 locus, leading to LMX1A controlled expression of BFP (Figure 1). Detailed description of CRISPR/Cas9 editing, associated genotyping and quality control analysis is provided in Supplemental methods and supplemental table 1 and 2.

2.3. Immunofluorescence

Cultures were fixed with 4% (w/v) paraformaldehyde and permeabilized with 0.1% (v/v) Triton X-100 in PBS (PBS-T). Following blocking with 1% (w/v) bovine serum albumin and 3% (v/v) donkey serum, cells were incubated with primary antibodies overnight at 4°C. After three washes with PBS-T, cells were incubated with complementary Alexa Fluor-conjugated antibodies (1:1000, Life technologies) for 1 hour at room temperature, and then counterstained with DAPI. All antibodies were diluted in PBS-T containing 1% BSA, 1% donkey serum. The primary antibodies used in the study are detailed in supplemental table 3.

Images were acquired using a Leica DMI600b inverted microscope. Cell counting was carried out using the CellProfiler (22) or FIJI (23) software to analyze 5-6 randomly placed fields of view per replicate. Data were collected from 3 independent differentiation runs for 2 clonal lines each, each with 2 technical replicates. The total sample size (n) is indicated in Figure legends.

2.4. Flow cytometry and FACS purification

For flow cytometry, cultured cells were dissociated with Accutase as described above and washed twice with DPBS by centrifugation at 900rpm for 5 minutes. Cells were resuspended in DPBS and passed through cell strainers with 35μm mesh (Corning) before being analyzed on a BD LSRFortessa™ cell analyzer. Data was analyzed in FlowJo (BD Biosciences).

For FACS purification, day 18 cultures were processed as described above but resuspended into a sorting buffer containing N2B27, 100ng/mL FGF8 and ROCK inhibitor Y-27632 (10μM, Tocris Bioscience). Sorting was performed on a BD FACSAria III using a 100 M nozzle. Background autofluorescence was compensated for using the KOLF2 parental cell line at the same stage of differentiation, this population was defined the BFP$^-$ gating. BFP$^+$ and BFP$^-$ cells were isolated using a highly restrictive gating strategy to exclude doublets and debris based on forward- and side-scatter parameters. FACS isolated cell fractions were replated at 250,000 cells/cm^2 for neuronal differentiation.

2.5. Single cell RNA sequencing (scRNAseq) and associated data analysis

Cells were dispensed at a concentration of 30000 cells/ml onto nanowells using the ICELL8 Single-Cell System (Takara). The cDNA libraries were generated using the

SMART-Seq ICELL8 cx Application Kit protocol provided by the manufacturer. Sequencing was carried out on Illumina HiSeq 4000 using 75bp paired-end sequencing with dual indexing (time course experiment) or the Illumina NovaSeq 6000 platform using 100bp paired-end sequencing with dual indexing (MPP^+ experiment). Raw sequencing data were processed using the Mappa pipeline v1.0 (Takara) and aligned to Homo sapiens GRCh38.99 primary assembly with the BFP reporter gene attached to the end of the genome. Counts including introns from the Mappa (1.0) pipeline to infer intron and exon counts as proxy of un-spliced and spliced RNAs for RNA velocity analysis using velociraptor R package. Downstream analysis was performed using Seurat R package. Detailed methods were described in the supplemental methods.

2.6. LDH-Glo™ Cytotoxicity and Annexin V/ dead cell apoptosis Assays

Neuronal cultures were treated with 1, 2.5 or 5 mM MPP^+ (D048, Sigma; prepared fresh following the manufacturer's instructions) or sterile water as vehicle. 24 h after treatment, supernatants were diluted 1:10 in storage buffer. LDH detection reagent and quantification was performed following the manufacturer's instruction (J2380, Promega). The essay was carried out using 3 technical replicates per culture well. Luminiscence was recorded after 45 minutes incubation at room temperature using a CLARIOstar plate reader (BMG Labtech) with the following optic settings: emission wavelength 580nm, emission bandwith 80nm, gain 3600 and focal heigh 10mm.

Annexin V dead cell assay was carried out using the Alexa fluor 488 Annexin V/Dead cell apoptosis kit (V13245, Invitrogen). Working reagents were prepared following the manufacturer's instructions. Cultures were washed with PBS and dissociate into single cells using Accutase for 10 min at 37°C followed by gently pipetting and another 2 minutes of incubation at 37°C. Accutase reaction was stopped using the same volume of media and the cells washed by centrifugation in PBS and re-suspended in 1X annexin-binding buffer. Cell suspension was then incubated with 5% (v/v) Alexa Fluor® 488 Annexin V and 10μg/mL PI at room temperature for 15 minutes. After this incubation period, 4 times the volume of 1X annexin-binding buffer was added. The stained cells were then processed using the BD LSRFortessa cell analyzer by measuring the fluorescence emission at 530 nm and 575 nm with the gating strategy shown in Figure S2 and data analyzed in FlowJo. The assays were performed in three independent cultures.

2.7 Statistical Analysis

Statistical analyses were performed using IBM SPSS 23 software. Student's t test or Mann-Whitney U test were used for comparisons between two groups. One-way ANOVA with Bonferroni Post Hoc or Kruskal-Wallis Test used for comparisons between three groups. Statistically significant differences were considered when p-value ≤ 0.05.

3. Results

3.1. Generation of human iPSC LMX1A-Cre/AAVS1-BFP lineage tracer line

The LMX1A-Cre/AAVS1-BFP tracer line was generated following two rounds of CRISPR/Cas9 genome editing in the KOLF2-C1 human iPSC line (to be referred to as KOLF2 subsequently): 1) knock-in a silent BFP expression unit into the AAVS1 (PPP1R12C) safe harbour locus; 2) targeted insertion of Cre recombinase coding sequence to the LMX1A gene immediately upstream of the stop codon (Figure 1A-B). With this design, Cre expression is dependent on that of endogenous LMX1A. Cre/LoxP mediated recombination in $LMX1A^+$ cells will lead to the removal of LoxP flanked promoter-less puromycin resistance cassette (PAC-pA) in the AAVS1 locus and hence activate BFP expression. Since genetic PAC-pA removal is inherited, BFP should be expressed in $LMX1A^+$ cells as well as their differentiated progeny.

For genome editing in the AAVS1 locus, plasmids containing the AAVS1 donor template and gRNA were electroporated into the KOLF2 cells. 40 puromycin resistant clones were isolated, expanded and genotyped by genomic PCR (Figure 1C-D) followed by

Sanger sequencing of candidate mutant PCR product. 74% of the clones analyzed had heterozygous BFP insertion (AAVS1$^{BFP/+}$) while 5% had BFP targeted in both alleles (homozygous BFP insertion, AAVS1$^{BFP/BFP}$, Figure 1E). For Cre knock-in into the LMX1A locus, the LMX1A donor template and gRNA were transfected to one of the homozygous BFP lines followed by G418 selection. 54 drug resistant colonies were picked and expanded clonally. PCR genotyping and Sanger sequencing (Figure 1C-D) identified 15 heterozygous (LMX1A$^{Cre/+}$) and 5 homozygous (LMX1A$^{Cre/Cre}$) Cre knock-in lines (Figure 1E).

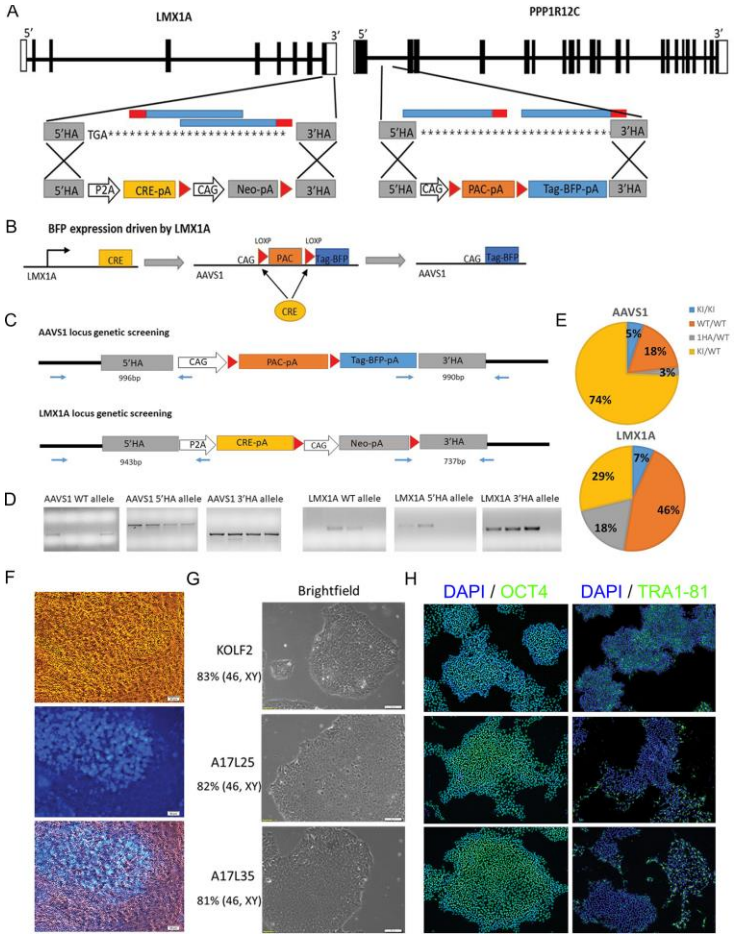

Figure 1. Generation of LMX1A-Cre/AAVS1-BFP tracing lines. (A) Schematic illustration of the wild type LMX1A and PPP1R12C (AAVS1) loci and targeting strategy. Exons are indicated as black rectangles. left: LMX1A targeting, the two gRNAs targeting the 3'UTR of LMX1A are indicated in blue with PAM region in red. The P2A-Cre-pA and Neo-pA expression cassettes are flanked by the homologous arms (HA) corresponding to exon 8 immediately upstream of the stop codon and 3'UTR (grey), respectively. Right: AAVS1 targeting, the two gRNAs targeting intron 1 of AAVS1 were indicated in blue with PAM region in red. The homologous arms (HA), indicated in grey, flank a PAC-pA selection cassette and BFP-pA fluorescent tag gene. (B) Mechanism of BFP activation driven by LMX1A expression. (C) Genomic PCR screening strategy for detecting the targeted clones at the AAVS1 and LMX1A locus, respectively. (D) Examples of agarose gels showing amplicons for the WT and HR allele. (E) Targeting efficiency for AAVS1 and LMX1A locus, respectively. (F) Bright field and fluorescent images of day 10 mDA differentiation cultures showing BFP expression in live cells. Scale bar 50µM. (G) Representative bright field images of iPSC colonies and (H) immunostaining of pluripotency markers OCT4 and TRA1-81 with DAPI counterstain for the parental KOLF2 and A17L25 and A17L35 LMX1ACre-BFP lines. Karyotyping results are indicated on the left below the corresponding iPSC lines.

As an initial test for Cre-driven BFP expression, two LMX1A homozygous (LMX1A$^{Cre/Cre}$, AAVS1$^{BFP/BFP}$) and two LMX1A heterozygous lines (LMX1A$^{Cre/+}$, AAVS1$^{BFP/BFP}$) were differentiated towards mDA fate and BFP expression monitored using live cell imaging and Flow cytometry (Figure 1F and Figure S1A-B). At day 30, the LMX1A

heterozygous cultures contained 40-60% BFP$^+$ cells. In contrast, less than 1% BFP$^+$ cells were detected in the LMX1A homozygous cultures (Figure S2B), suggesting that homozygous Cre knock-in in the LMX1A locus may be deleterious to LMX1A expressing cells. Therefore, the two LMX1A$^{Cre/+}$, AAVS1$^{BFP/BFP}$ lines, A17L25 and A17L35, were used for the subsequent studies. For simplicity, these two lines were also referred to as L25 and L35 individually in figures and in general as the LMX1A-Cre/AAVS1-BFP tracer lines. As undifferentiated cells, both cell lines exhibited characteristic pluripotent stem cell morphology, expressed pluripotency markers OCT4, SOX2 and TRA1-81 (Figure 1G-H). Moreover, more than 80% metaphases analyzed were of normal karyotype (46, XY) (Figure 1G) and no new copy number variances were detected compared to the parental KOLF2 iPSC cells (Table S2).

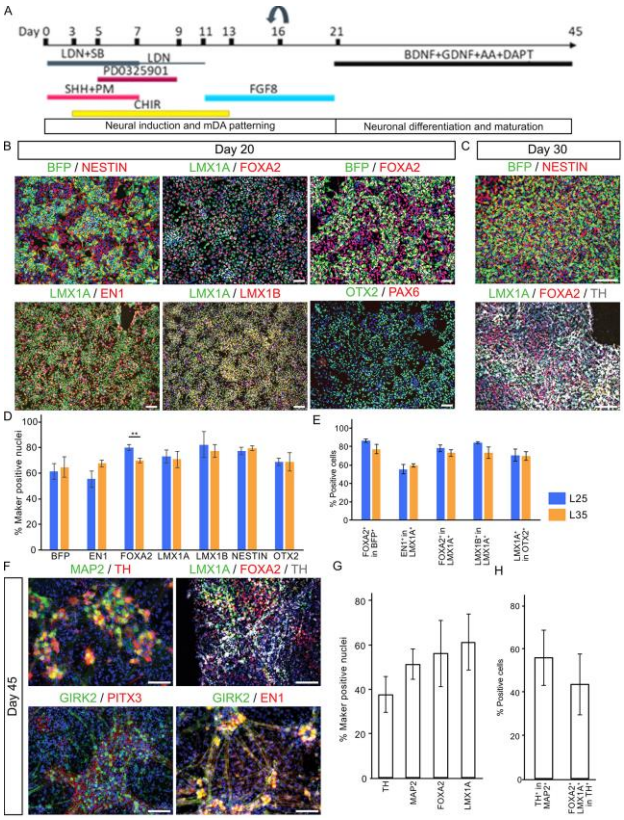

Figure 2. Immunocytochemical characterization of mDA cultures. (A) Illustrations of mDA differentiation protocol. (B) Shown are representative day 20 cultures stained for antibodies against BFP, NESTIN, LMX1A, FOXA2, EN1, LMX1B, OTX2 and PAX6. (C) Day 30 cultures immunostained for BFP, NESTIN, LMX1A, FOXA2 and TH. (D-E) Bar graph showing quantitative representation of the above, data are presented as mean ± SD of three independent differentiation. Student's t test was employed for comparison between A17L25 and A17L35 for each measurement. None but FOXA2 was significantly different between the two lines (P=0.009, **). (F) Day 45 cultures immunostained for LMX1A, FOXA2, EN1, GIRK2, MAP2, PITX3 and TH. (G) Bar graph showing quantification of day 45 immunostaining. Scale bar 100μM.

3.2. Immunocytochemistry and flow cytometry characterization of LMX1A-Cre/AAVS1-BFP derived mDA cultures

We next examined mDA differentiation capacity of L25 and L35 lines using a protocol optimized from Jaeger and Kirks (2, 3) followed by immunocytochemical analysis of major mDA lineage markers and the BFP tracer (Figure 2A). At day 20, cultures derived from both cell lines were highly enriched with cells expressing the pan-neural progenitor marker NESTIN and transcription factors expressed in the ventral midbrain and/or playing important roles in mDA fate specification such as LMX1A, FOXA2, OTX2, EN1 and LMX1B (Figure 2B, 2D) (16, 18, 19, 24-27). BFP protein was detected in over 60% of the

cells. Around 80-90% of LMX1A⁺ and BFP⁺ cells co-expressed FOXA2, respectively, suggesting a very high correlation between BFP and LMX1A expression (Figure 2E). In contrast, PAX6, a dorsal forebrain marker gene that is also expressed in the lateral midbrain neural progenitors, was barely detected (Figure 2B). These observations confirmed the highly efficient production of ventral midbrain progenitors.

As cultures progressed to day 30, tyrosine hydroxylase (TH) expressing cells became evident, indicating the production of postmitotic DA neurons at this stage (Figure 2C). By day 45, cells expressing other postmitotic mDA neuronal markers (Figure 2F-G), such as PITX3 and GIRK2 were readily detectable while expression of LMX1A and FOXA2 are largely maintained in mDA neurons as demonstrated by co-expression with TH (Figure 2H) (28, 29).

A prospective application of the LMX1A-Cre/AAVS1-BFP tracer line is the isolation of mDA progenitors and their differentiated derivatives for studies that benefit from a pure population of mDA linage. We therefore tested FACS purification of BFP⁺ cells at day 18 of L25 and L35 differentiation (Figure 3A). Immunostaining for LMX1A showed that 95.40±0.15% of replated sorted BFP⁺ cultures were LMX1A⁺ (Figure 3B-C). Three days after FACS purification, the sorted BFP⁺ cultures contained around 30% more LMX1A⁺ cells than the non-sorted sister control cultures (L25, P=0.005; L35, P= 0.001), approximately 10% more NESTIN⁺BFP⁺ (L25 P= 0.0316; L35 P= 0.013), and 20% increase of NESTIN⁺LMX1A⁺ cells (L25 P= 0.005; L35 P= 0.001) (Figure 3D-E). At 38 days post-sorting (ie. day 56 of differentiation), we detected a similar proportion of BFP⁺ cells in the sorted BFP⁺ derived cultures compared to that of day 18 (Figure 3F-G) and was approximately 30% higher than that in the non-sorted cultures (L25, P= 0.00023; L35 P= 0.0032) (Figure 3F-G).

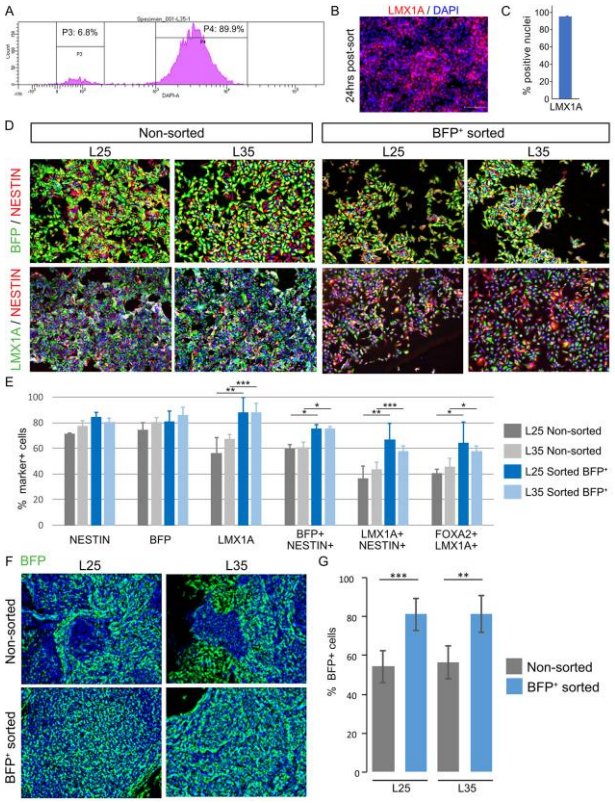

Figure 3. Enrichment of mDA cultures by FACS of BFP⁺ neural progenitors. (A) An example of FACS Aria histogram of BFP negative and positive gates for sorting L25 day18 mDA neural progenitors. (B). LMX1A antibody staining of sorted BFP⁺ cells 24 hours post FACS. (C) Bar graph showing the quantitative representation of the above. (D) Representative images of immunostaining for BFP, NESTIN and LMX1A in non-sorted control and sorted BFP⁺ cultures 3 days post-FACS. (E) Bar graphs showing quantitative representation of the above. (F) BFP antibody staining of non-sorted and sorted BFP⁺ cultures 38 days post FACS (ie. 56 days of total culture time). BFP stained in green, DAPI in blue. (G) Bar

graph showing quantification of the above, Data represent mean ± SD of 3 independent cultures performed with each of the two cell lines. (* p≤0.05, ** p≤0.01, *** p≤0.001).

3.3. Single cell transcriptomic analysis confirms the generation of bona fide mDA neurons.

To further evaluate mDA cultures derived from the LMX1A-Cre/AAVS1-BFP tracer lines, we employed the ICELL8 platform and the full-length SMART-Seq2 technology to study the transcriptomic profile of individual cells at days 21, 30, 45 and 65 of differentiation. Of the total 776 qualifying cells (185 at d21, 272 at d30, 78 at d45 and 232 at d65), we detected 13402 protein coding genes with an average of 5800 genes per cell. Principal component analysis using the top 5000 most variable genes identified seven unbiased cluster cells (C0 to C6 based on cell numbers, Figure 4A, 4C). Cells of d21, d30 were strongly segregated from each other and those of d45 and d65, which were clustered closely together (Figure 4B). Accordingly, we detected a greater number of differentially expressed genes (DEGs) between d21 and d30 and between d30 and d45, respectively, compared to DEGs between d45 and d65 (Wilcoxon Test, Padj< 0.05, log2FC > 0.25, Figure 4D-E). Notably, we detected few DEGs between derivatives of the two tracing lines (Figure 4E, Figure S3A-C), demonstrating a high level of consistency and reproducibility of our lines and differentiation paradigm.

We annotated the cell clusters based on the expression of known gene markers (Figure 4D). C3 and C5 contained mainly d21 progenitor cells and were characterized by high expression of midbrain floor plate marker CORIN and basal progenitor marker HES1, as well as other early mDA progenitor genes such as SOX6, LMX1A, LMX1B, OTX2, FOXA1 and FOXA2 (7, 30). C0 and C4 showed high expression of TOP2A that marks mitotic chromosomes and cycling cell marker MKI67 (Ki67), and a higher expression of mDA progenitor markers EN1 and EN2 compared to other clusters. C1, C2 and C6 were made up of d45 and d65 cells, C6 was assigned as astrocytic lineage due to their expression of SOX9, SLC1A3 (EAAT1) and S100B. C1 and C2 were characterized as DA neurons based on their broad expression of neuronal gene SYT1 in addition to several dopaminergic markers including TH, CALB1, RET, PBX1, SLC18A1 (VMAT1) and SLC6A3 (DAT). However, C2 shows a highly enriched expression of SNAP25, suggesting a more mature neuronal state. To corroborate the cluster annotation, we analyzed our data using the transcriptional profile of 'neuronal progenitors', 'neuroblast' and 'dopaminergic neurons' from the human embryonic midbrain (hEM) as reference (31). Indeed, our progenitor clusters (C0, 3, 4 and 5), were predicted as neuronal progenitors while C1and C2 were mapped to a mix of neuroblasts and dopaminergic neurons (Figure 4F, Figure S3F).

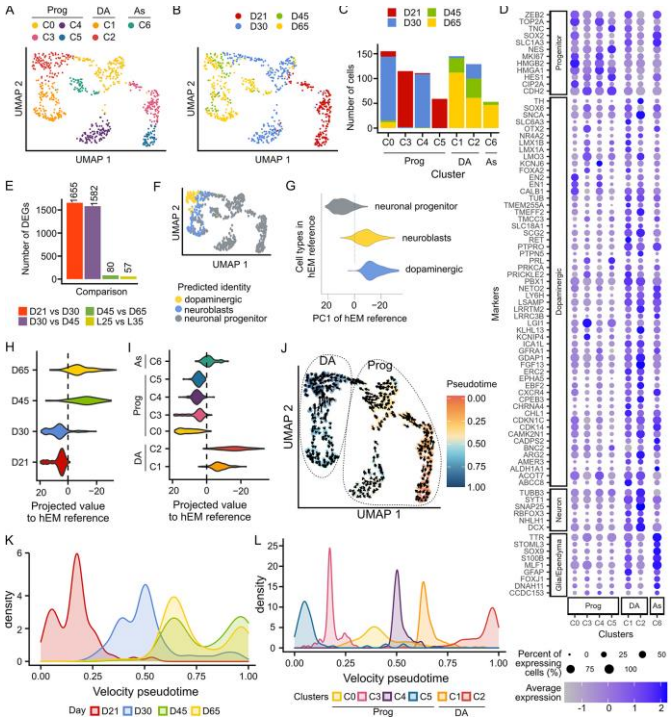

Figure 4. Transcriptional profiling of in vitro differentiation of iPSC into DA neurons. (A) UMAP plot colored by the cell clusters identified using the first 10 principal components and the top 5000 most variable features across 767 cells. (B) UMAP plot colored by differentiation day showing strong temporal segregation, particularly between d21 and d30. (C) Bar graph showing the number of cells per cluster and the distribution of cells from each time point. (D) Dot plot of known class defying markers that aided the annotation of cell clusters (E) Bar plot illustrating the number of DEGs between cells of different stages of differentiation and between the two tracer lines. DEGs were identified by a Wilcoxon test, adjusted p value < 0.05. (F) UMAP shows the predicted cell type using the human embryonic midbrain (hEM) as reference. (G) Violin plot illustrating the separation of neuronal progenitors, neuroblasts and dopaminergic neurons along the first principal component PC1 in the reference developing human midbrain dataset (PMID 27716510). In the hEM we observed that PC1 segregates progenitors (negative PC1 values) from dopaminergic neurons (positive PC1 values), the violin plot shows the projection of our cells into PC1 grouped by differentiation day in (H) and cell cluster in (I). (J) RNA velocity projected on top of UMAP shows the current and predicted (arrowhead) transcriptional states of cells. Cells are colored by pseudotime, which has been calculated based on RNA velocity across the top 5000 most variable genes and indicates the transition states between cells. (K) Density plot shows the distribution of cells by differentiation day along pseudotime. (L). Density plot showing the distribution of cells by cluster along pseudotime.

We noticed that the first principal component (PC1) of the hEM separated neuronal progenitors (positive PC1 values) from neuroblasts and dopaminergic neurons (negative PC1 values, Figure 4G). Thus, we projected our scRNA-seq time course gene expression data into the same PC1 and observed a strong segregation of d21 and d30 cells from d45 and d65 cells, which projects closer to where hEM neuroblasts and dopaminergic neurons lie (Figure 4H). PC1 projection also supports the more mature nature of C2 compared to C1 (Figure 4I). Finally, we calculated the RNA velocity of these cells, a method that examines the ratio of unspliced/spliced mRNA for predicting the future state of individual cells and hence the directionality of the differentiation trajectory (Figure 4J)(31). Applying RNA velocity to individual cells within C0-5, we observed even better segregation between cells of differentiation of d45 and d65 cells from d21 or d30 cells (Figure 4K). Consistent with principal component projection and reference mapping results, RNA velocity trajectory analysis demonstrates that C2 is more mature than C1 and other progenitor populations (Figure 4L).

Taken together, our scRNAseq analysis confirmed efficient generation of ventral midbrain progenitors and postmitotic mDA neurons using the optimized differentiation

paradigm. Moreover, d45 mDA neurons exhibit similar transcriptomic profiles to those at d65.

3.4. Preferential sensitivity of BFP⁺ neurons to MPP⁺ toxicity

1-Methyl-4-phenyl-1,2,5,6-tetrahydropyridine (MPTP) or its metabolite methyl-4-phenylpyridinium (MPP^+) are known to selectively damage mDA neurons and produce symptoms that resemble those observed in Parkinson's disease (PD). To demonstrate the relevance of our iPSC-derived mDA neurons in PD modelling, we tested MPP^+ cytotoxicity to d45 cells by quantifying the release of lactate dehydrogenase (LDH) to the culture media as a measure of cell death. After 24 hour treatment with or without 1, 2.5 and 5mM MPP^+, we detected significant increase of LDH in cultures treated with 2.5 and 5mM MPP^+ (Figure 5A). To complement the above, we performed a cytometry based Annexin V binding assay. Combing with propidium Iodide (PI) staining, this assay distinguishes live, dead (necrotic) and apoptotic cells. We found a significant decrease in the proportions of viable cells (P=0.001), representing approximately 35% reduction of total live cells in the 2.5 and 5mM MPP^+ treatment conditions. Concurrent with the decreased number of live cells, we observed an increase in the proportions of necrotic cells (P=0.009) across all MPP^+ doses in comparison with the vehicle controls (Figure 5B). Interestingly, parallel quantification of BFP^+ cells of these cultures revealed a progressive decrease of this population with increasing MPP^+ dosage (P=0.001) (Figure 5C). The ~50% reductions of BFP^+ cells under 2.5 and 5mM MPP^+ conditions were greater than that of total live cells in the same treated cultures, suggesting that BFP^+ neurons (ie. derivative of LMX1A neural progenitors) are preferentially vulnerable to MPP^+ toxicity.

To substantiate the above findings, we performed scRNAseq analysis on d45 cells treated with or without 1mM MPP^+ for 24 hours. Both the vehicle control (basal) and MPP^+ treated groups included non-sorted (NS) d45 cells and d45 cells derived from d18 sorted BFP^+ and BFP^- cell fractions. The basal and MPP^+ treated cells were clearly segregated (Figure 5D), while segregation by sorting status was less prominent overall except populations of d18 sorted BFP^- fraction (Figure 5E). We first identified six clusters among all cells from the basal condition samples, which segregated mainly into progenitors (B2, B4, B5) and neurons (B0, B1, B3, Figure 5F-G, Figure S4A). We observed segregation by their sorting status such that B3 were largely composed of derivatives of sorted BFP^+ cells whereas B0 was mainly made up of BFP^- fraction (Figure 5F, Figure S4A-B). B1 and B3 cells exhibit mDA transcriptomics characteristics, with B3 cells more mature than B1 as exemplified by their richer expression of SNAP25 and SYT1 (Figure 5G). In contrast, B0 cluster express higher levels of, or contains a greater proportion of cells within the cluster that express genes not compatible with DA neurons (eg. STT, SLC17A6/7, ISL1). Using the basal clusters as reference, we next predicted the identity of MPP^+ treated cells (Figure 5F, Figure S4C-E) and compared the proportion of each cluster between the basal and MPP^+ conditions using a permutation test (Figure 5F, Figure S5). Among the neuronal clusters, only the B3 DA cluster showed a significant reduction in the after MPP^+ exposure (FDR < 0.001998), implying preferential sensitivity of B3 neurons.

We next performed differential expression analysis in the neuronal B3 population between the MPP^+ and basal conditions. Despite the small number of B3 cells obtained following the MPP^+ treated condition, we were able to identify 78 DEGs (adjusted p value < 0.05, supplementary table 4-6). Gene Ontology enrichment analyses were separately performed with the up regulated (n = 28) and down regulated genes (n = 50). The biological pathways enriched in the up regulated genes include intrinsic apoptotic signaling while down regulated pathways include oxidative phosphorylation, consistent with the mitochondrial toxicity of MPP^+ and also implicated role of one-carbon metabolism in neurodegeneration (32,33) (Figure 5I, J). Together, our transcriptomic analysis provide support that a fraction of BFP^+ neurons are particularly sensitive to MPP+ cytotoxicity.

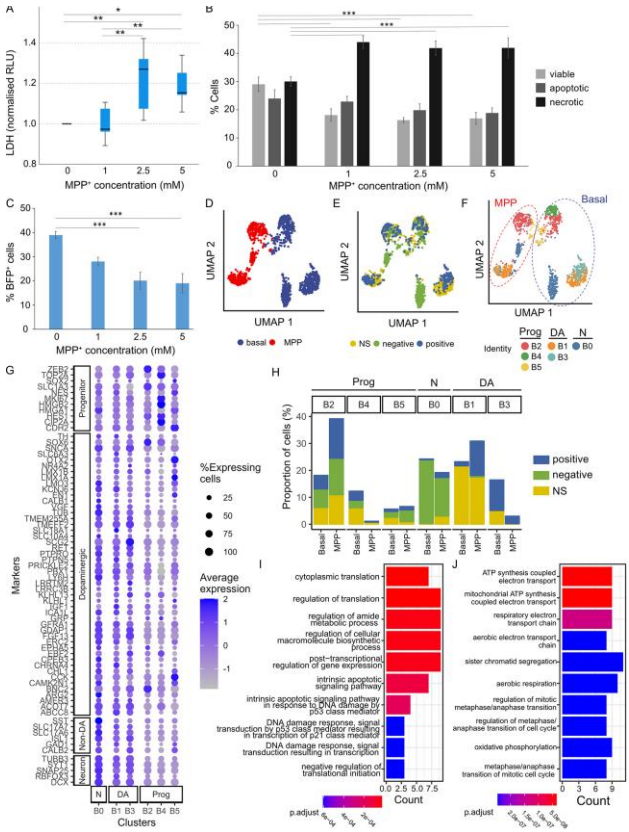

Figure 5. Modelling PD-related toxicity using MPP⁺. (A) Quantification of MPP⁺ cytotoxicity by LDH assay. Kruskal-Wallis H Test, P= 0.003, Pairwise comparisons: 0mM vs 1mM, P=0.797, 0mM vs 2.5mM, P=0.008, 0mM vs 5mM, P=0.020, 1mM vs 2.5mM, P=0.004, 1mM vs 5mM, P=0.010, 2.5mM vs 5mM, P=0.838. (B) Quantification of viable, apoptotic and necrotic cells determined by Annexin V assay. ANOVA, P=0.001 for viable cells; P=0.009 for necrotic fraction. (C) Increasing doses of MPP⁺ led to progressive decrease of BFP⁺ cells. ANOVA, P=0.001. Data shown in A-C represents mean ± s.e.m. from 3 biological replicates each with 3 technical replicates per condition of two independent cell lines. * p≤0.05, ** p≤0.01, *** p≤0.001. (D) UMAP plot showing strong segregation of untreated (basal) and MPP⁺ treated cells (a total of 1418 cells). (E) UMAP plot including basal and MPP⁺ treated cells colored by sorted status (BFP⁺, BFP⁻ and NS). (F) UMAP plot colored by clusters identified for the basal cells (B0 to B5) and predicted clusters of MPP⁺ treated cells using the basal cell profile as reference. (G) Dot plot showing the expression of marker genes in different clusters of both basal and MPP⁺-treated cells. (H) Bar graph showing the distribution and portion of cells in each of the 6 clusters, which are presented separated by the sorting status. (I-J) Top 10 gene ontologies (GO) enriched in the DEGs upregulated (I) and downregulated (J) in MPP⁺ treated B3 population compared to basal B3 population.

4. Discussion

Using CRISPR/Cas9 assisted knock-in of Cre and BFP in the LMX1A and AAVS1 loci, respectively, we successfully generated LMX1A-Cre/AAVS1-BFP tracer lines for labelling hiPSC-derived LMX1A⁺ mDA neural progenitors and their differentiated neuronal progenies. We showed, via immunocytochemical analysis and single cell transcriptomic profiling, that BFP⁺ cells co-expressed LMX1A and cardinal mDA neural progenitor markers at the neural progenitor stage of in vitro differentiation, which progress into postmitotic TH⁺ dopamine neurons as differentiation progressed. The mDA progenitors were amenable to FACS purification and subsequent differentiation into postmitotic dopaminergic neurons.

Initially demonstrated in mouse ESCs via knocking GFP into the Pitx3 locus (34), a number of PSC lines have been reported to date for sorting DA neurons. These sorting systems are based on targeted insertion of a reporter into a gene with restricted expression pattern in the mDA lineage (PITX3 or LMX1A) (35, 36) or expressed in all DA neurons (eg.

TH)(37). The reporters in these tools mirror the expression of their target genes in real time so cells isolated using these systems are target gene expressing cells at the time of sorting. The LMX1A-Cre/AAVS1-BFP tracer line reported here differs from those tools in that BFP is expressed in cells expressing LMX1A at the time of analysis as well as progeny of LMX1A$^+$ cells that themselves may no longer expressing LMX1A. Since LMX1A expression is downregulated in a subpopulation of mDA neurons and does not cover the entire mDA neuronal popula (31, 38), the LMX1A-Cre/AAVS1-BFP line would have an advantage over the LMX1A-GFP knock-in line for isolating postmitotic mDA neurons, as the PITX3-GFP system. Another application of the LMX1A tracing system which cannot be fulfilled by postmitotic reporter system, such as PITX3- or TH- based knock-in, is for lineage tracing studies. For example, to investigate potential regional characteristics of glial cells derived from LMX1A$^+$ floor plate progenitors.

Several cell surface markers have been identified for isolating ventral midbrain neural progenitors which include CORIN (39), TPBG (40); LRTM1(41) amongst others (42-44). Cell surface marker-based purification has advantages over genetic based approach as it can be readily applied to all PSC lines. It was reported that TPBG$^+$ cells contains ~50% of LMXA$^+$FOXA2$^+$ cells while LRTM1 sorting enriched LMX1A$^+$FOXA2$^+$ cells to 77.2±2.1%. Thus new cell surface markers may be needed to cover the whole spectrum of mDA progenitors.

Our scRNAseq profiling of d21-65 cultures and integrated analysis with that of the human fetal ventral midbrain demonstrates that our iPSC-derived cell populations corresponded very well to progenitors and dopaminergic neurons of the hEM (31), providing unbiased confirmation of their mDA progenitor and neuronal identities. Interestingly, while morphological maturation continued to progress in culture from d45 onwards, we found that d45 and d65 cells were very similar at transcriptional level. This finding suggests that for studies that primarily measure transcriptomics changes, for instance, high throughput drug or gene screening via scRNAseq, one could save 20 days in vitro culture by using d45 mDA neurons.

By modelling PD-related drug toxicity using MPP$^+$, we found that the dose dependent increase of cell death and decrease of total live cell cells is accompanied by a greater reduction in the proportion of BFP$^+$ neurons within the same MPP$^+$ treated cultures, hence demonstrating preferential susceptibility of BFP$^+$ neurons to MPP$^+$ toxicity. Interestingly, single cell transcriptomic analysis of MPP$^+$ treated neurons derived from d18 sorted BFP$^+$ and BFP$^-$ neural progenitors and non-sorted sister cultures revealed the biggest degree of cell loss being the B3 cluster, which contains mostly of d18 sorted BFP$^+$ fraction with essentially no contribution from the sorted BFP$^-$ fraction. Together, these findings strongly support the relevance of using BFP$^+$ neurons for studying PD-related damage and vulnerability.

Attempts were made to provide insights into potential transcriptomics characteristics of MPP$^+$ sensitive B3 neurons by comparing gene expression between the basal and MPP$^+$ treated B3 cells. This had proved challenging as it was difficult to discern whether the DGEs detected were driven by cell identity or from their response to MPP$^+$. Further scRNAseq with greater number of cells at basal and MPP$^+$ treated condition may help to reveal heterogeneity within the B3 population and allow the identification of BFP$^+$ sensitive subpopulations and their molecular characteristics without compounding effects of MPP$^+$ regulated gene expression.

5. Conclusion

In summary, this work established a new tool to study human midbrain dopaminergic neuron development and a more refined model to study PD-related toxicity and investigations into PD etiology in combinations with CRISPR/CAS9 genome editing of associated risk genes. As a tracer line, the LMX1A-Cre/AAVS1-BFP iPSC cells can provide an unique opportunity for investigations into differentiated derivatives of midbrain floor plate progenitors beyond mDA neurons.

Supplementary Materials: The following supporting information can be downloaded at: www.mdpi.com/xxx/s1, Supplementary methods, Figure S1-S4, Table S1-S3.

Author Contributions: C.W. M.L. and L.F.C. conceived the study and M.L. and L.F.C designed the targeting constructs for generating the BFP tracer lines. L.F.C. carried out and analyzed all cell experiments and data interpretation with assistance from Z.L. J.M.S. performed scRNAseq data analysis and Z. L. helped with some figure preparation. C. W. provided financial support. M.L. L.F.C. and J.M.S. wrote the paper. All authors commented on the manuscript.

Funding: This work was supported by the UK Dementia Research Institute to C.W. (MC_PC_17112) which receives its funding from the UK DRI Ltd, funded by the UK Medical Research Council, Alzheimer's Society and Alzheimer's Research UK. Z.L. was funded by a UK Dementia Research Institute PhD studentship.

Institutional Review Board Statement: Not applicable.

Informed Consent Statement: Not applicable.

Data Availability Statement: The sequencing data discussed in this publication have been deposited in NCBI's Gene Expression Omnibus (Edgar et al., 2002) and are accessible through GEO Series accession number GSE247600 and GSE249360. Code is available at GitHub (https://github.com/jmonzon87/LMX1A_iPSC_DA).

Acknowledgments: We thank all members of the C. W. and M.L. laboratories for helpful discussions during the course of this study. Thanks also to Ms. J. Morgan and A. Evans, M. Rockiki and M. Bishop for technical assistance. Part of this work was performed using the computational facilities of the Advance Research Computing at Cardiff (ARCCA) Division, Cardiff University.

Conflicts of Interest: The authors declare no conflict of interest.

References

1. Poewe W, Seppi K, Tanner CM, Halliday GM, Brundin P, Volkmann J, et al. Parkinson disease. Nat Rev Dis Primers. 2017;3:17013.

2. Kriks S, Shim JW, Piao J, Ganat YM, Wakeman DR, Xie Z, et al. Dopamine neurons derived from human ES cells efficiently engraft in animal models of Parkinson's disease. Nature. 2011;480(7378):547-51.

3. Jaeger I, Arber C, Risner-Janiczek JR, Kuechler J, Pritzsche D, Chen IC, et al. Temporally controlled modulation of FGF/ERK signaling directs midbrain dopaminergic neural progenitor fate in mouse and human pluripotent stem cells. Development. 2011;138(20):4363-74.

4. Nolbrant S, Heuer A, Parmar M, Kirkeby A. Generation of high-purity human ventral midbrain dopaminergic progenitors for in vitro maturation and intracerebral transplantation. Nat Protoc. 2017;12(9):1962-79.

5. Kirkeby A, Grealish S, Wolf DA, Nelander J, Wood J, Lundblad M, et al. Generation of regionally specified neural progenitors and functional neurons from human embryonic stem cells under defined conditions. Cell Rep. 2012;1(6):703-14.

6. Denham M, Bye C, Leung J, Conley BJ, Thompson LH, Dottori M. Glycogen synthase kinase 3beta and activin/nodal inhibition in human embryonic stem cells induces a pre-neuroepithelial state that is required for specification to a floor plate cell lineage. Stem Cells. 2012;30(11):2400-11.

7. Doi D, Samata B, Katsukawa M, Kikuchi T, Morizane A, Ono Y, et al. Isolation of human induced pluripotent stem cell-derived dopaminergic progenitors by cell sorting for successful transplantation. Stem Cell Reports. 2014;2(3):337-50.

8. Drummond NJ, Singh Dolt K, Canham MA, Kilbride P, Morris GJ, Kunath T. Cryopreservation of Human Midbrain Dopaminergic Neural Progenitor Cells Poised for Neuronal Differentiation. Front Cell Dev Biol. 2020;8:578907.

9. Marton RM, Ioannidis JPA. A Comprehensive Analysis of Protocols for Deriving Dopaminergic Neurons from Human Pluripotent Stem Cells. Stem Cells Transl M

10. Xia N, Fang F, Zhang P, Cui J, Tep-Cullison C, Hamerley T, et al. A Knockin Reporter Allows Purification and Characterization of mDA Neurons from Heterogeneous Populations. Cell Rep. 2017;18(10):2533-46.

11. Fiorenzano A, Birtele M, Wahlestedt JN, Parmar M. Evaluation of TH-Cre knock-in cell lines for detection and specific targeting of stem cell-derived dopaminergic neurons. Heliyon. 2021;7(1):e06006.

12. Rakovic A, Voss D, Vulinovic F, Meier B, Hellberg AK, Nau C, et al. Electrophysiological Properties of Induced Pluripotent Stem Cell-Derived Midbrain Dopaminergic Neurons Correlate With Expression of Tyrosine Hydroxylase. Front Cell Neurosci. 2022;16:817198.

13. Sandor C, Robertson P, Lang C, Heger A, Booth H, Vowles J, et al. Transcriptomic profiling of purified patient-derived dopamine neurons identifies convergent perturbations and therapeutics for Parkinson's disease. Hum Mol Genet. 2017;26(3):552-66.

14. Zambon F, Cherubini M, Fernandes HJR, Lang C, Ryan BJ, Volpato V, et al. Cellular alpha-synuclein pathology is associated with bioenergetic dysfunction in Parkinson's iPSC-derived dopamine neurons. Hum Mol Genet. 2019;28(12):2001-13.

15. Grimm J, Mueller A, Hefti F, Rosenthal A. Molecular basis for catecholaminergic neuron diversity. Proc Natl Acad Sci U S A. 2004;101(38):13891-6.

16. Andersson E, Tryggvason U, Deng Q, Friling S, Alekseenko Z, Robert B, et al. Identification of intrinsic determinants of midbrain dopamine neurons. Cell. 2006;124(2):393-405.

17. Ono Y, Nakatani T, Sakamoto Y, Mizuhara E, Minaki Y, Kumai M, et al. Differences in neurogenic potential in floor plate cells along an anteroposterior location: midbrain dopaminergic neurons originate from mesencephalic floor plate cells. Development. 2007;134(17):3213-25.

18. Deng Q, Andersson E, Hedlund E, Alekseenko Z, Coppola E, Panman L, et al. Specific and integrated roles of Lmx1a, Lmx1b and Phox2a in ventral midbrain development. Development. 2011;138(16):3399-408.

19. Yan CH, Levesque M, Claxton S, Johnson RL, Ang SL. Lmx1a and lmx1b function cooperatively to regulate proliferation, specification, and differentiation of midbrain dopaminergic progenitors. J Neurosci. 2011;31(35):12413-25.

20. Hildebrandt MR, Reuter MS, Wei W, Tayebi N, Liu J, Sharmin S, et al. Precision Health Resource of Control iPSC Lines for Versatile Multilineage Differentiation. Stem Cell Reports. 2019 10(6):1126-1141.

21. Arber C, Precious SV, Cambray S, Risner-Janiczek JR, Kelly C, Noakes Z, et al. Activin A directs striatal projection neuron differentiation of human pluripotent stem cells. Development. 2015;142(7):1375-86.

22. Stirling DR, Swain-Bowden MJ, Lucas AM, Carpenter AE, Cimini BA, Goodman A. CellProfiler 4: improvements in speed, utility and usability. BMC Bioinformatics. 2021;22(1):433.

23. Schindelin J, Arganda-Carreras I, Frise E, Kaynig V, Longair M, Pietzsch T, et al. Fiji: an open-source platform for biological-image analysis. Nat Methods. 2012;9(7):676-82.

24. Broccoli V, Boncinelli E, Wurst W. The caudal limit of Otx2 expression positions the isthmic organizer. Nature. 1999;401(6749):164-8.

25. Millet S, Bloch-Gallego E, Simeone A, Alvarado-Mallart RM. The caudal limit of Otx2 gene expression as a marker of the midbrain/hindbrain boundary: a study using in situ hybridisation and chick/quail homotopic grafts. Development. 1996;122(12):3785-97.

26. Ferri AL, Lin W, Mavromatakis YE, Wang JC, Sasaki H, Whitsett JA, et al. Foxa1 and Foxa2 regulate multiple phases of midbrain dopaminergic neuron development in a dosage-dependent manner. Development. 2007;134(15):2761-9.

27. Simon HH, Saueressig H, Wurst W, Goulding MD, O'Leary DD. Fate of midbrain dopaminergic neurons controlled by the engrailed genes. J Neurosci. 2001;21(9):3126-34.

28. Nunes I, Tovmasian LT, Silva RM, Burke RE, Goff SP. Pitx3 is required for development of substantia nigra dopaminergic neurons. Proc Natl Acad Sci U S A. 2003;100(7):4245-50.

29. Schein JC, Hunter DD, Roffler-Tarlov S. Girk2 expression in the ventral midbrain, cerebellum, and olfactory bulb and its relationship to the murine mutation weaver. Dev Biol. 1998;204(2):432-50.

30. Liang L, Tian Y, Feng L, Wang C, Feng G, Stacey GN, et al. Single-cell transcriptomics reveals the cell fate transitions of human dopaminergic progenitors derived from hESCs. Stem Cell Res Ther. 2022;13(1):412.

31. La Manno G, Gyllborg D, Codeluppi S, Nishimura K, Salto C, Zeisel A, et al. Molecular Diversity of Midbrain Development in Mouse, Human, and Stem Cells. Cell. 2016;167(2):566-80.e19.

32. Murray LK, Jadavji NM. The role of one-carbon metabolism and homocysteine in Parkinson's disease onset, pathology and mechanisms. Nutr Res Rev. 2019; 32(2):218.

33. Lionaki E. Ploumi C. Tavernarakis N. One-Carbon Metabolism: Pulling the Strings behind Aging and Neurodegeneration. Cells. 2022; 11(2):214.

34. Maxwell SL, Ho HY, Kuehner E, Zhao S, Li M. Pitx3 regulates tyrosine hydroxylase expression in the substantia nigra and identifies a subgroup of mesencephalic dopaminergic progenitor neurons during mouse development. Dev Biol. 2005;282(2):467-79.

35. Watmuff B, Hartley BJ, Hunt CP, Fabb SA, Pouton CW, Haynes JM. Human pluripotent stem cell derived midbrain PITX3(eGFP/w) neurons: a versatile tool for pharmacological screening and neurodegenerative modeling. Front. Cell Neurosci 2015; 9:104.

36. de Luzy IR, Niclis JC, Gantner CW, Kauhausen JA, Pouton C, Hunt C et al. An LMX1a-GFP expressing human pluripotent stem cell line, but not PITX3-GFP, enables isolation and enrichment of dopaminergic progenitors targeted at improved cell replacement therapy for Parkinsonian Disease. J Neurosci. 2019; pii: 1160-19.

37. Calatayud C, Carola G, Fernández-Carasa I. et al. CRISPR/Cas9-mediated generation of a tyrosine hydroxylase reporter iPSC line for live imaging and isolation of dopaminergic neurons. Sci Rep. 2019; 9:6811.

38. Asgrimsdottir ES, Arenas E. Midbrain Dopaminergic Neuron Development at the Single Cell Level: In vivo and in Stem Cells. Front Cell Dev Biol. 2020; 8:463.

39 Ono Y, Nakatani T, Sakamoto Y, Mizuhara E, Kumai M, Kamaguchi A et al., Differences in neurogenic potential in floor plate cells along an anteroposterior location: midbrain dopaminergic neurons originate from mesencephalic floor plate cells. Development. 2007; 134(17):3213-25.

40. Yoo JE, Lee DR, Park S, Shin HR, Lee KG, Kim DS et al. Trophoblast glycoprotein is a marker for efficient sorting of ventral mesencephalic dopaminergic precursors derived from human pluripotent stem cells. NPJ Parkinsons Dis. 2021; 7(1):61.

41. Samata B, Doi D, Nishimura K, Kikuchi T, Watanabe A, Sakamoto Y. et al. Purification of functional human ES and iPSC-derived midbrain dopaminergic progenitors using LRTM1. Nat Commun. 2016; 7:13097.

42. Gennet N, Tamburnni C, Nan X, Li, M. FolR1: a novel cell surface marker for isolating midbrain dopamine neural progenitors and nascent dopamine neurons. Scientific Reports. 2016; 6:32488.

43. Fathi A, Mirzaei M, Dolatyar B, Sharifitabar M, Bayat M, Shahbazi E, et al. Discovery of Novel Cell Surface Markers for Purification of Embryonic Dopamine Progenitors for Transplantation in Parkinson's Disease Animal Models. Mol Cell Proteomics. 2018; 17(9):1670-84.

44. Xu P, He H, Gao Q, Zhou Y, et al. Human midbrain dopaminergic neuronal differentiation markers predict cell therapy outcomes in a Parkinson's disease model. J Clin Invest. 2022; 132(14): e156768.